Pergamon

Int. J. Multiphase Flow Vol. 24, No. 4, pp. 539–561, 1998

Printed in Great Britain
PII: S0301-9322(97)00074-8
0301-9322/98 $19.00 + 0.00

THEORETICAL ANALYSIS OF FLOW CHARACTERISTICS OF MULTIPHASE MIXTURES IN A VERTICAL PIPE

NATSUO HATTA[1], HITOSHI FUJIMOTO[1], MAKOTO ISOBE†[2] and JUNG-SEOCK KANG[3]

[1]Graduate School of Energy Science, Kyoto University, Kyoto, 606-8501, Japan
[2]Graduate Student, Kyoto University, Kyoto, 606-8501, Japan
[3]Korea Institute of Geology, Mining & Materials, Yusung, Taejon, 305-600, Korea

(Received 6 April 1997; in revised form 5 October 1997)

Abstract—This paper is concerned with the theoretical analysis to obtain the flow characteristics of multiphase mixtures in a vertically fixed air-lifting pipe. In this present investigation, the case is treated where a transition process from a solid–liquid two-phase mixture flow to a solid–gas–liquid three-phase mixture by injecting gas-phase into the upriser through a gas injector is present. The system of equations governing the liquid–solid two-phase mixture flow consists of two mass conservation equations, two momentum conservation equations and a requirement for two phase volumetric fractions. Again, the gas–liquid–solid three-phase flow field after the position of gas injection is solved by three mass conservation equations, three momentum equations, a gas equation of state and a requirement for the individual phase volumetric fractions. The transitions of the flow pattern of gas phase from bubbly to slug flows and from slug to churn flows are taken into account in the system of equations governing the three-phase flows. In order to verify the validity of the system of governing equations accounting for the flow patterns transitions of gas-phase, the flow characteristics calculated on the basis of the present theoretical model have been compared with experimental data measured by the other investigators. As a result, we have found that the present theoretical model built up in this study gives a good fit to the experimental data obtained by several investigators. Furthermore, we have demonstrated that the present model is capable of predicting the maximum solid/liquid volumetric flux.

Key Words: air-lift pump, theoretical analysis, transitions of flow pattern, two- and three-phase flows, flow characteristics

1. INTRODUCTION

It is very difficult to theoretically analyze the flow characteristics of the case where two or three different phases, among solid-, gas- and liquid-phases, interact with each other and such two- or three-phase mixtures flow in a pipe. It is commonly accepted that the situation where the flow field peculiar to the mixture flow can be concretely solved without relying on any empirical/experimental constitutive equation is restricted to the equilibrium/homogeneous two-phase flow capable of neglecting the velocity difference between different phases.

The air-lift pump, which was originally thought to be applicable for a few simple uses like pumping water, has been utilized as a means of conveying slurries in mining and transporting explosive/poisonous liquid. More recently, it has been reported by Kamata and Ito (1995) that in the steel making process, although the principle of the air-lift pump is applied only to an RH vacuum degasser to circulate molten steel and to remove hydrogen gas, carbon and unmetallic inclusions in molten steel, the simplicity of the equipment may make it applicable for the transportation of molten iron/steel between different refining processes. Again, it is well known that there are a vast amounts of marine mineral resources such as manganese nodules at the deep-sea bed of 4000 m to 6000 m in water depth. For lifting these mineral ores from the deep-sea bed to the sea surface, the utilization of the air-lift pump is anticipated and examined from various aspects.

†Present address: Engineer, Oita Works, Nippon Steel Corp., Oita 870, Japan

Thus, Yoshinaga *et al* (1990, 1996) proposed a method for predicting the steady operation performance by applying the momentum conservation law to a control volume bounded by the wall and the top and bottom cross sections of the lifting pipe. This is based upon a very simple principle of the mechanics such that the difference between the momentum which leaves through the top cross section and the momentum which enters through the bottom cross section corresponds to the external forces; the friction force acting between the pipe wall and the mixture, the body force of gravity and the pressure force of the surrounding water acting on the bottom cross section. They compared the predicted results on the basis of the method with the experimental data by other investigators and their own experimental data and confirmed the validity. Also, they pointed out that none of the methods proposed by other investigators can give good fit to the experiments performed by Sadatomi *et al.* (1990a). However, it is unbelievable that their method is omnipotent due to the fact that the idea which underlies their method is too simple. In fact, they themselves (1990b) recognized that at very high air flow rates, the predicted values on the basis of the method are lower by about 30% at maximum than the experimental ones. Also, it is impossible to treat the unsteady problems by their method.

Now, it seems to be very difficult to establish an economically optimum condition for operation performance of air-lift pump, since the theoretical model to predict the flow characteristics has been not exactly built up yet. It may be commonly accepted that one of the main factors which make it extremely difficult is the transitions of the flow pattern of gas-phase. When gas–liquid mixtures flow upward in a vertical pipe, the two phases distribute in a number of patterns, each characterizing the radical and/or axial distribution of liquid and gas. The flow is usually quite chaotic, and these phase distributions are difficult to describe. Hewitt and Hall-Taylor (1970) designate four basic patterns for upflow namely, bubbly flow, slug flow, churn flow and annular flow. In the case of annular flow, the continuity of the gas along the pipe appears in the core. Accordingly, the solid particles can not be conveyed upward when the transition to the annular flow occurs in a vertical long pipe.

A multifluid model is generally formulated by a set of conservation equations governing the balance of mass, momentum and energy of each phase. Since the macroscopic fields of one phase are not independent of those of the other phases, the interaction terms which couple the transport of mass, momentum, and energy of each phase across the interface appear in the field equation. In the multifluid model formulation, the transport processes of each phase are expressed by their own balance equations. Therefore, it can be expected that the model can predict more detailed changes and phase interactions than a mixture model such as the drift flux model, see Zuber (1967) and Ishii (1977). As pointed out by Ishii (1982), the weakest link in the multifluid model formulation is the constitutive equations for the interfacial interaction terms, and the difficulties arise due to the complicated motion and transitions of the flow pattern of gas-phase, as mentioned already. It is indispensable to introduce constitutive relations for interfacial transfer terms, in particular, the drag correlation and interfacial area concentration for each flow pattern into the multifluid model formulation.

The purpose of the present investigation is to theoretically analyze the flow characteristics of the air-lift pump for the case where a transitional process from the solid–liquid two-phase mixture flow to the solid–gas–liquid three-phase mixture one by injecting gas-phase into the upriser through a gas-injector is present. The system of governing equations is based upon the multifluid model. Therefore, the equations governing the two-phase mixture flow consist of two mass conservation equations, two momentum equations and an equation for the solid and liquid volumetric fractions. Also, the solid–gas–liquid three-phase mixture flow field after the position of the gas-injector is solved by three mass conservation equations, three momentum conservation equations, a gas equation of state and an equation for the individual phase volumetric fractions. The transitions of the flow pattern of gas-phase from the bubble flow to the slug flow and the slug flow to the churn flow are taken into account in the system of equations governing the three-phase mixture flow. In order to verify the validity of the system of equations accounting for flow pattern transitions, the flow characteristics calculated on the basis of the present theoretical model have been compared with the experimental data measured by several other investigators and discussed from various aspects.

2. GOVERNING EQUATIONS

In this present investigation, the system of equations governing the solid–liquid two-phase and the solid–gas–liquid three-phase flows is based upon the multifluid model. The body of the air-lift pump consists of two parts. One of which is a suction pipe where the solid–liquid two-phase mixture flows. The other is the upriser where the solid–gas–liquid three-phase mixture flows. Therefore, the system of equations should be classified into two parts: (1) the solid–liquid two-phase flow region from the bottom cross section to the position of the gas injection and (2) solid–gas–liquid three-phase flow region from the position of the gas injection to the top cross section. In the two-phase region, the number of the flow characteristics to be required is five factors (u_L, u_S, ε_L, ε_S, and P). In the three-phase region, the number is eight factors (u_G, u_L, u_S, ε_G, ε_L, ε_S, P and ρ_G). Here, u, ε, P and ρ denote the velocity, volumetric fraction, pressure and density, respectively. The subscripts G, L and S denote the gas-, liquid- and solid-phases, respectively. On the other hand, the system of equations governing the two-phase mixture flow consists of two mass conservation equations, two momentum conservation equations and an equation for volumetric fraction requirement. Also, the system of equations governing the mixture flow in the upriser is composed of three mass conservation equations, three momentum conservation equations, a gas equation of state and an equation for volumetric fraction requirement. The system of equations is mathematically closed both in the two- and three-phase regions.

Prior to the description of the system of governing equations, we wish to define the coordinate system along the vertical lifting pipe. Figure 1 shows the outline of the mixture flow system along the vertical and straight pipe with a uniform cross sectional area. x denotes the distance from the bottom end of the pipe ($x = 0$). The position of gas injection is set at $x = L_g$ and the position of the top end of the pipe corresponding to the upriser outlet is set at $x = L$. The distance from the bottom end to the water surface level is denoted by L_s ($< L$). Accordingly, the range of $0 \leq x < L_g$ corresponds to the solid–liquid two-phase flow region and the range of $L_g \leq x \leq L$ corresponds to the solid–gas–liquid three-phase flow region along the x-axis.

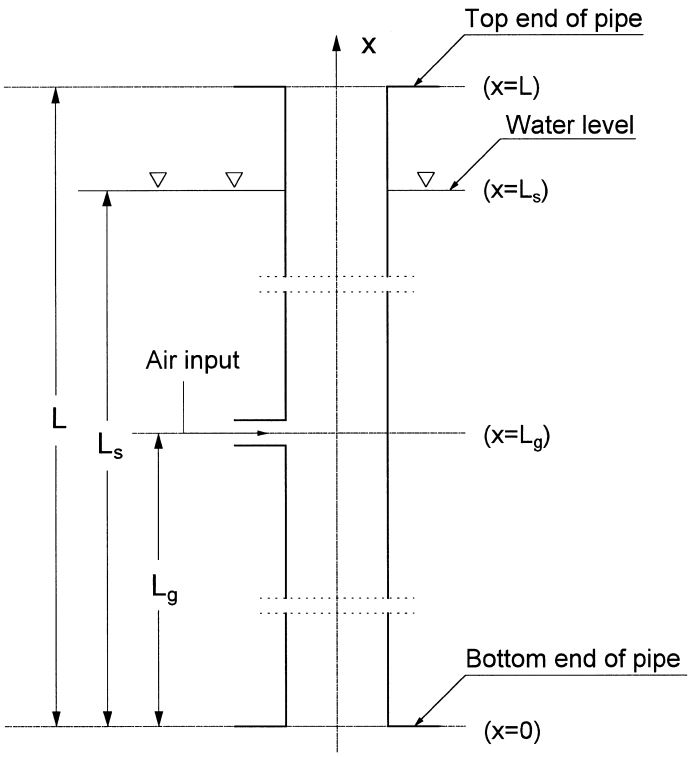

Figure 1. Outline of mixture flow system in a vertical pipe.

The conservation equations of mass and momentum which govern each phase in the solid–gas–liquid three-phase flow region are given by

$$\frac{\partial(\rho_G \epsilon_G)}{\partial t} + \frac{\partial(\rho_G \epsilon_G u_G)}{\partial x} = 0 \quad [1]$$

$$\frac{\partial(\rho_L \epsilon_L)}{\partial t} + \frac{\partial(\rho_L \epsilon_L u_L)}{\partial x} = 0 \quad [2]$$

$$\frac{\partial(\rho_S \epsilon_S)}{\partial t} + \frac{\partial(\rho_S \epsilon_S u_S)}{\partial x} = 0 \quad [3]$$

$$\frac{\partial(\rho_G \epsilon_G u_G)}{\partial t} + \frac{\partial(\rho_G \epsilon_G u_G^2)}{\partial x} = -\left(F_{iG} + F_{wG} + F_{gG} + F_{vG} + \epsilon_G \frac{\partial P}{\partial x}\right) \quad [4]$$

$$\frac{\partial(\rho_L \epsilon_L u_L)}{\partial t} + \frac{\partial(\rho_L \epsilon_L u_L^2)}{\partial x} = -\left(F_{iL} + F_{wL} + F_{gL} + F_{vL} + \epsilon_L \frac{\partial P}{\partial x}\right) \quad [5]$$

$$\frac{\partial(\rho_S \epsilon_S u_S)}{\partial t} + \frac{\partial(\rho_S \epsilon_S u_S^2)}{\partial x} = -\left(F_{iS} + F_{wS} + F_{gS} + F_{vS} + \epsilon_S \frac{\partial P}{\partial x}\right) \quad [6]$$

in which t is the time. F_{ik} (k = G, L, S) appearing in the momentum conservation equations denotes the drag force transferred to phase k (per unit volume) due to the interaction between phases. F_{wk} is the friction force transferred from pipe wall to phase k. F_{gk} is the gravity force acting to phase k and F_{vk} is the virtual mass force acting to phase k in accelerating multi-phase flow.

And the following relations

$$P = \rho_G RT \quad [7]$$

$$\epsilon_G + \epsilon_L + \epsilon_S = 1 \quad [8]$$

must be satisfied. Here, R is the gas constant and T is the absolute temperature of gas-phase. T is regarded as constant because the mixture flow field is assumed to be in thermal equilibrium between/among phases and the temperature gradient is neglected along the lifting pipe. Since the volumetric fraction of solid-phase is very small compared with that of gas-phase in the operation performance of air-lift pump, the interaction will be neglected between solid- and gas-phases.

The system of equations governing the solid–liquid two-phase mixture flow can be easily obtained by putting $\varepsilon_G = 0$ and $F_{iG} = F_{wG} = F_{gG} = F_{vG} = 0$ in [1]–[8]. At the same time, the gas equation of state given by [7] is not required in the solid–liquid flow region. Therefore, as mentioned above, the five flow characteristics to be required in this region can be determined by the five governing equations.

However, in order to practically evaluate the flow characteristics of the mixture flow, it is indispensable to formulate the external forces acting to phase k (F_{ik}, F_{wk}, F_{gk} and F_{vk}) appearing in [4]–[6]. Furthermore, the key issue in the accurate modelling of multiphase flow is to specify the constitutive terms, which includes the phase interaction terms. The closure relationship used in the present theoretical model will be described in the next section.

3. FORMULATION OF EXTERNAL FORCES AND INTERACTIVE EFFECTS

3.1. *Drag force*

The drag force depends on the pressure distribution acting on a material surface being in liquid-phase and the interfacial friction owing to slip between solid- and liquid-phases and/or between gas- and liquid-phases.

Firstly, the drag $F_{i\mathrm{G}}$ transferred from liquid-phase to gas-phase is given by

$$F_{i\mathrm{G}} = \frac{1}{8}\rho_{\mathrm{L}} a_{i\mathrm{G}} C_{D\mathrm{G}} |u_{\mathrm{G}} - u_{\mathrm{L}}|(u_{\mathrm{G}} - u_{\mathrm{L}}) \quad [9]$$

in which $a_{i\mathrm{G}}$ and $C_{D\mathrm{G}}$ denote the interfacial area concentration and the drag coefficient, respectively. These depend upon the flow patterns of gas-phase strongly. Since the interfacial area concentration is a parameter which characterizes the structure of a flow, its mechanistic modelling is based upon the geometrical factors, gas volumetric fraction and flow. According to Ishii *et al.* (1982), the interfacial area per unit volume is given as follows,

$$a_{i\mathrm{G}} = a_{i\mathrm{G}b} = \frac{6\epsilon_{\mathrm{G}}}{d_{sm}} \quad [10]$$

in the bubble flow regime and

$$a_{i\mathrm{G}} = a_{i\mathrm{G}s} = \frac{4.5}{D}\frac{\epsilon_{\mathrm{G}} - \epsilon_{\mathrm{G}s}}{1 - \epsilon_{\mathrm{G}s}} + \frac{6\epsilon_{\mathrm{G}s}}{d_{sm}}\frac{1 - \epsilon_{\mathrm{G}}}{1 - \epsilon_{\mathrm{G}s}} \quad [11]$$

in the slug and churn-turbulent flow regimes. Here, the D is the pipe diameter. $\varepsilon_{\mathrm{G}s}$ and d_{sm} denote the average gas volumetric fraction in the liquid slug and the sauter mean diameter of small bubbles in the liquid slug, respectively. The first term on the right hand side in [11] represents the contribution of the gas slug and the second term is that of small bubbles in the liquid slug. Kurul and Podowski (1991) recommended the following expression for $\varepsilon_{\mathrm{G}s}$

$$\epsilon_{\mathrm{G}s} = \begin{cases} \epsilon_{\mathrm{G}} & (0 < \epsilon_{\mathrm{G}} < 0.25) \\ 0.3929 - 0.5714\epsilon_{\mathrm{G}} & (0.25 \le \epsilon_{\mathrm{G}} < 1) \\ 0.05 & (0.6 \le \epsilon_{\mathrm{G}} < 1) \end{cases} \quad [12]$$

According to this, the interfacial area concentration calculated by [11] agrees with the expression of [10] in the region of $0 < \varepsilon_{\mathrm{G}} < 0.25$ and it is suggested that the flow pattern corresponds to the bubble flow regime.

Again, the following relation,

$$d_{sm} = 1.06\left(\frac{\sigma}{\rho_{\mathrm{L}}^{1/3}}\right)^{1/3}\left\{\frac{\epsilon_{\mathrm{G}}(1 - \epsilon_{\mathrm{G}})D^2}{j(-\mathrm{d}P/\mathrm{d}x)}\right\}^{2/9} \quad [13]$$

is given by Kocamustafaogullari *et al.* (1994). Here, σ is the surface tension and j is the superficial velocity which is represented by the sum of the volumetric fluxes of solid-, gas- and liquid-phases ($j = j_{\mathrm{G}} + j_{\mathrm{L}} + j_{\mathrm{S}}$).

We consider the flow pattern transitions of gas-phase when the mixture containing the gas-phase flows upward in a vertical pipe. Griffith and Wallis (1961) postulated that the bubble–slug transition depends on the gas volumetric fraction ε_{G} and the criterion for transition from bubbly to slug flow is that ε_{G} reaches 0.25 or a little more. This agrees with the prediction by Kurul and Podowski (1991) who recommended that the interfacial area concentration $\varepsilon_{\mathrm{G}s} = \varepsilon_{\mathrm{G}}$ (see [12]) can be used for volumetric fraction ε_{G} less than 0.25. Taitel *et al.* (1980) also supported this value for the bubble-slug transition.

Denoting the gas volumetric fraction by ε_1 when the transition to the slug flow begins to occur and by ε_2 when the transition to the slug flow reaches completion, we assume in the present investigation that

$$\epsilon_1 = 0.25 - 0.05 \quad [14]$$

$$\epsilon_2 = 0.25 + 0.05 \quad [15]$$

Also, denoting the volumetric fraction by ε_1 when the slug–churn transition begins to happen and by ε_2 when the transition to the churn flow is just concluded, we assume that

$$\epsilon_1 = 0.7415 - 0.05 \quad [16]$$

$$\epsilon_2 = 0.7415 + 0.05 \quad [17]$$

This value, 0.7415, is determined, as will be mentioned later, by regarding the drag coefficient of the slug flow to be equal to that of the churn flow, because the drag coefficient is given as a function of the gas volumetric fraction in the two regimes. In the transitional regions from the bubbly to the slug flows and the slug to the churn flows, the following weight factor,

$$r = \frac{1}{2}\left\{1 + \sin\left[\frac{\pi}{2}\left(\frac{2\epsilon_G - \epsilon_1 - \epsilon_2}{\epsilon_2 - \epsilon_1}\right)\right]\right\} \quad [18]$$

is introduced to the interpolation of the interfacial area concentration.

For the transition range from the bubbly to the slug flows,

$$a_{iG} = (1 - r)a_{iGb} + ra_{iGs} \quad [19]$$

and for the transition range from the slug to the churn flows,

$$a_{iG} = (1 - r)a_{iGs} + ra_{iGc} \quad [20]$$

are introduced to the calculation to be mentioned later. However, the weight factor r for the transition from the slug to the churn flows becomes substantially meaningless, because the expression of the interfacial area concentration shown by [11] is given in the same form for both the slug and the churn flows. At any rate, a width for the transition region is designated in the present theoretical model on the premise that the transition of the gas flow pattern does not discontinuously occur, but it continuously occurs.

The interfacial drag coefficient of gas-phase, of course, is different depending upon the gas flow pattern. The drag coefficient, C_{DGb}, for a swarm of bubbles

$$C_{DGb} = \frac{C_{DG0}}{\sqrt{\epsilon_L}} \quad [21]$$

is proposed by Tomiyama *et al.* (1995a,b). Here, since $C_{DGb} \simeq C_{DG0}$ if $\varepsilon_L \simeq 1$, C_{DG0} denotes the drag coefficient of a single bubble in a stagnant liquid and is given by

$$C_{DG0} = \max\left(\min\left[\frac{24}{Re_G}(1 + 0.15Re_G^{0.687}), \frac{72}{Re_G}\right], \frac{8}{3}\frac{E_0}{E_0 + 4}\right) \quad [22]$$

in which Re_G and E_0 denote the bubble Reynolds number and the Eötvös number, respectively, and are defined by

$$Re_G = \frac{d_G|u_G - u_L|\rho_L}{\mu_L} \quad [23]$$

$$E_0 = \frac{g(\rho_L - \rho_G)d_G^2}{\sigma} \quad [24]$$

Here the d_G is assumed to be d_{sm} (see [13]). It has been reported that [22] is applicable under the conditions of $10^{-3} < Re_G < 10^5$, $10^{-2} < E_0 < 10^3$ and $10^{-14} < M < 10^7$, in which M is the Morton number defined as

$$M = \frac{g\mu_L^4(\rho_L - \rho_G)}{\rho_L^2\sigma^3} \quad [25]$$

Furthermore, the interfacial drag coefficient of the slug flow C_{DGs} and that of the churn flow C_{DGc} are given by

$$C_{DGs} = 9.8(1 - \epsilon_b)^3 \quad [26]$$

$$C_{DGc} = \frac{8}{3}(1 - \epsilon_b)^2 \quad [27]$$

respectively (Ishii *et al*. 1982). Here,

$$\epsilon_b = \frac{\epsilon_G - \epsilon_{Gs}}{1 - \epsilon_{Gs}} \quad [28]$$

In the present theoretical model, for the transition range from the bubbly to the slug flows,

$$C_{DG} = (1 - r)C_{DGb} + rC_{DGs} \quad [29]$$

and for the transition range from the slug to the churn flows

$$C_{DG} = (1 - r)C_{DGs} + rC_{DGc} \quad [30]$$

where the weight factor r is the same as defined in [18].

By the way, we can understand that the value of 0.7415 appearing in [16] and [17] corresponds to the gas volumetric fraction of the case where the drag coefficient of the slug flow is set to be equal to that of the churn flow, as already mentioned.

Since the solid particles to be lifted are incompressible and their shape remains unchangeable along a vertical pipe, the interfacial area concentration a_{iS} is given by

$$a_{iS} = \frac{6\epsilon_S}{d_S} \quad [31]$$

in which d_S is the diameter when the solid particles are spherical in shape. If otherwise, d_S is the diameter of equivalent sphere after reduction on the assumption that the particles are spherical body with the same volume and density. Therefore, the interfacial drag force F_{iS} per unit volume exerted by the liquid-phase to the solid particle is given by

$$F_{iS} = \frac{3}{4}\frac{\epsilon_S}{d_S}\rho_L C_{Ds}|u_S - u_L|(u_S - u_L) \quad [32]$$

Also, the drag coefficient of solid particles is evaluated as a function of the particle Reynolds number by

$$C_{DS} = \begin{cases} \dfrac{24}{Re_S}(1 + 0.15Re_S^{0.687}) & (Re_S \leq 700) \\ \left[\sqrt{\dfrac{24}{Re_S}} + 0.34\left(Re_S^{0.06} + \dfrac{1}{1.72 + 0.018Re_S}\right)\right]^2 & (700 < Re_S < 1.5 \times 10^5) \end{cases} \quad [33]$$

when the particles are spherical in shape. Here, Re_S is defined by

$$Re_S = \frac{d_S|u_S - u_L|\rho_L}{\mu_L} \quad [34]$$

If the particles are not spherical, we can experimentally evaluate the drag coefficient from the power balance on condition that the terminal velocity is reached in a stagnant liquid.

The interfacial drags F_{iG} and F_{iS} exerted to the gas- and solid-phases, respectively are based upon the interaction with the liquid-phase. Accordingly, the following relation

$$F_{iG} + F_{iL} + F_{iS} = 0 \quad [35]$$

holds between/among different phases.

3.2. *Frictional force between mixture and pipe wall*

When two- and three-phase mixture flows upward in a vertical pipe, the pressure drop occurs owing to interfacial friction between the mixture and the inner wall of pipe. In the present model, the gas–pipe wall friction and the solid particles–pipe wall friction are neglected, and the friction force is apparently represented by the liquid–pipe wall interaction. Therefore, the friction forces, F_{wk} (k = G, L, S), described in [4]–[6] are put as

$$F_{wG} = 0 \quad [36]$$

$$F_{w\mathrm{L}} = \frac{\mathrm{d}P_f}{\mathrm{d}x} = -\frac{1}{2}\lambda\rho_m u_m^2 \frac{1}{D} \quad [37]$$

$$F_{w\mathrm{S}} = 0 \quad [38]$$

in which ρ_m is the mixture density given by

$$\rho_m = \epsilon_{\mathrm{L}}\rho_{\mathrm{L}} + \epsilon_{\mathrm{S}}\rho_{\mathrm{S}} \quad [39]$$

in the solid–liquid two-phase flow region and

$$\rho_m = \epsilon_{\mathrm{G}}\rho_{\mathrm{G}} + \epsilon_{\mathrm{L}}\rho_{\mathrm{L}} + \epsilon_{\mathrm{S}}\rho_{\mathrm{S}} \quad [40]$$

in the solid–gas–liquid three–phase region. Also, u_m denotes the superficial mixture velocity given by

$$u_m = \epsilon_{\mathrm{L}}u_{\mathrm{L}} + \epsilon_{\mathrm{S}}u_{\mathrm{S}} \quad [41]$$

in the solid–liquid two-phase mixture flow region and

$$u_m = \epsilon_{\mathrm{G}}u_{\mathrm{G}} + \epsilon_{\mathrm{S}}u_{\mathrm{S}}. \quad [42]$$

in the solid–gas–liquid three-phase mixture region. The friction factor λ needed in estimating the friction force can be predicted by the Blasius type equation based upon the superficial mixture velocity u_m and the liquid kinematic viscosity v_{L}, that is

$$\lambda = C\left(\frac{u_m D}{v_{\mathrm{L}}}\right)^{-n} \quad [43]$$

In the calculations to be compared with the experimental data measured by other investigators, as will be mentioned later, C and n are taken as 0.45 and $\frac{1}{5} \sim \frac{1}{4}$, respectively.

3.3. *Body force*

Since only the body force owing to the gravity may be taken into consideration, the body force terms, F_{gk} (k = G, L, S), appearing in [4]–[6] are simply expressed as

$$F_{g\mathrm{G}} = \epsilon_{\mathrm{G}}\rho_{\mathrm{G}}g \quad [44]$$

$$F_{g\mathrm{L}} = \epsilon_{\mathrm{L}}\rho_{\mathrm{L}}g \quad [45]$$

$$F_{g\mathrm{S}} = \epsilon_{\mathrm{S}}\rho_{\mathrm{S}}g \quad [46]$$

in which g denotes the acceleration due to the gravity.

3.4. *Virtual mass force*

The virtual mass force comes into play, when one phase is accelerating relative to the other. Lahey *et al.* (1980) investigated the effect of the virtual mass in accelerating gas–liquid two-phase flow for various nozzle/diffuser flows. The most general form of the one-dimensional and steady-state virtual mass acceleration a_{vm} is given by Drew *et al.* (1979)

$$a_{vm} = u_{\mathrm{G}}\frac{\mathrm{d}u_{\mathrm{G}}}{\mathrm{d}x} - u_{\mathrm{G}}\frac{\mathrm{d}u_{\mathrm{L}}}{\mathrm{d}x} + \mathrm{W}_v\left\{(\lambda_v - 2)(u_{\mathrm{G}} - u_{\mathrm{L}})\frac{\mathrm{d}u_{\mathrm{G}}}{\mathrm{d}x} + (1 - \lambda_v)(u_{\mathrm{G}} - u_{\mathrm{L}})\frac{\mathrm{d}u_{\mathrm{L}}}{\mathrm{d}x}\right\} \quad [47]$$

for the gas-phase in the gas–liquid two-phase flow. Here, λ_v and w_v are the arbitrary parameters to be determined experimentally.

Lahey *et al.* (1980) confirmed from the results of hypothetical nozzle/diffuser experiments for vertical co-current and counter-current flows that for the general a_{vm} case, with $\lambda_v = 1$ and $\lambda_v = 2$, very little difference in the calculated gas velocity u_{G} is evident, and that the answer is approximately unchanged, even when the virtual mass force is set to zero. From such a point of view, it is controversial whether or not the virtual mass force term need be introduced to the momentum

conservation equations for each phase. Then, the virtual mass force terms for gas-phase as well as solid-phase are given by

$$F_{v\mathrm{G}} = \epsilon_{\mathrm{G}}\rho_{\mathrm{L}}k_{v\mathrm{G}}\left\{\frac{\partial u_{\mathrm{G}}}{\partial t} - \frac{\partial u_{\mathrm{L}}}{\partial t} + u_{\mathrm{G}}\frac{\partial u_{\mathrm{G}}}{\partial x} - u_{\mathrm{G}}\frac{\partial u_{\mathrm{L}}}{\partial x} + w_V\left[(\lambda_v - 2)(u_{\mathrm{G}} - u_{\mathrm{L}})\frac{\partial u_{\mathrm{G}}}{\partial x} + (1-\lambda_v)(u_{\mathrm{G}} - u_{\mathrm{L}})\frac{\partial u_{\mathrm{L}}}{\partial x}\right]\right\} \quad [48]$$

$$F_{v\mathrm{S}} = \epsilon_{\mathrm{S}}\rho_{\mathrm{L}}k_{v\mathrm{S}}\left(\frac{\partial u_{\mathrm{S}}}{\partial t} - \frac{\partial u_{\mathrm{L}}}{\partial t} + u_{\mathrm{S}}\frac{\partial u_{\mathrm{S}}}{\partial x} - u_{\mathrm{L}}\frac{\partial u_{\mathrm{L}}}{\partial x}\right) \quad [49]$$

in which $k_{v\mathrm{G}}$ and $k_{v\mathrm{S}}$ denote the virtual mass coefficients of gas- and solid-phases, respectively, and are given by

$$k_{v\mathrm{G}} = \begin{cases} \frac{1}{2}\cdot\frac{1+2\epsilon_{\mathrm{G}}}{1-\epsilon_{\mathrm{G}}} & (0 \le \epsilon_{\mathrm{G}} < 0.5) \\ \frac{1}{2}\cdot\frac{3-2\epsilon_{\mathrm{G}}}{\epsilon_{\mathrm{G}}} & (0.5 \le \epsilon_{\mathrm{G}} < 1) \end{cases} \quad [50]$$

$$k_{v\mathrm{S}} = 0.5 \quad [51]$$

The constitutive equation [50] has been developed by Ransam *et al.* (1981) and we use this formula in the calculation to be mentioned later. Following Hinze (1962) and Wallis (1969), w_v is set to zero in the numerical calculations to be compared to the experiments performed by other investigators.

Since the virtual mass forces $F_{v\mathrm{G}}$ and $F_{v\mathrm{S}}$ exerted to the gas- and solid-phases, respectively, are based upon the interaction with the liquid-phase, the following balance law between different phases

$$F_{v\mathrm{G}} + F_{v\mathrm{L}} + F_{v\mathrm{S}} = 0 \quad [52]$$

should be obeyed.

4. PROCEDURE OF NUMERICAL CALCULATIONS

4.1. *Steady-state flow characteristics*

The procedure of numerical calculation on the steady-state condition is very simple and based upon numerical process mentioned in our previous works (Hatta and Fujimato 1996 and Fujimoto *et al.* 1997). Firstly, the gas and solid volumetric fractions $\varepsilon_{\mathrm{G}3}$,$\varepsilon_{\mathrm{S}3}$ just after of a gas-injector and the volumetric fluxes $j_{\mathrm{G}3}$, j_{L} and j_{S} are given, in which the suffix 2 and 3 denote the condition (or state) just before and after the gas-injector, respectively. In doing this, the flow characteristics in the solid–liquid two-phase mixture flow region can be determined as follows:

$$\epsilon_{\mathrm{L}3} = 1 - \epsilon_{\mathrm{G}3} - \epsilon_{\mathrm{S}3} \quad [53]$$

$$\epsilon_{\mathrm{L}2} = \frac{\epsilon_{\mathrm{L}3}}{(1-\epsilon_{\mathrm{G}3})} \quad [54]$$

$$\epsilon_{\mathrm{S}2} = 1 - \epsilon_{\mathrm{L}2} \quad [55]$$

$$u_{\mathrm{L}2} = \frac{j_{\mathrm{L}}}{\epsilon_{\mathrm{L}2}} \quad [56]$$

$$u_{\mathrm{S}2} = \frac{j_{\mathrm{S}}}{\epsilon_{\mathrm{S}2}} \quad [57]$$

Since all of the flow characteristics in the solid–liquid two-phase mixture flow region have been determined at this stage, the static pressure P_3 at the gas-injector can be obtained by

$$P_3 = P_0 - \rho_{m2} g L_g - \frac{1}{2}\lambda \rho_{m2} (j_L + j_S)^2 \frac{L_g}{D} \quad [58]$$

in which P_0 is the static pressure at the cross section of the suction pipe inlet at $x = 0$ (see figure 1). The gas density ρ_{G3} is given by the gas equation of state as

$$\rho_{G3} = \frac{P_3}{RT} \quad [59]$$

And the rising velocity for each phase just after the position of gas injection

$$u_{S3} = \frac{u_{S2}}{1 - \epsilon_{G3}} \quad [60]$$

$$u_{L3} = \frac{u_{L2}}{1 - \epsilon_{G3}} \quad [61]$$

$$u_{G3} = \frac{M_G}{A\epsilon_{G3}\rho_{G3}} = \frac{j_{Ga}\rho_{Ga}}{\epsilon_{G3}\rho_{G3}} \quad [62]$$

in which M_G is the gas-phase mass flow rate which is constant in the range of $L_g \leq x \leq L$. A denotes the cross section area of the pipe and j_{Ga} and ρ_{Ga} are the volumetric flux and density of the gas-phase. The subscript a denotes the value at the cross section of the upriser outlet.

By the above-mentioned numerical manipulation, the eight flow characteristics (ε_{G3}, ε_{L3}, ε_{S3}), (u_{G3}, u_{L3}, u_{S3}), P_3 and ρ_{G3} have been determined at this stage. Therefore, the system of equations governing the solid–gas–liquid three-phase mixture flow field is numerically solved as the boundary condition at $x = L_g$ with the above eight flow characteristics. Then, [4]–[6] are rewitten in a simple form of

$$\frac{dP}{dx} = C_1 + C_2 \frac{du_G}{dx} \quad [63]$$

$$\frac{du_L}{dx} = (A_1 + A_3 C_1) + (A_2 + A_3 C_2) \frac{du_L}{dx} \quad [64]$$

$$\frac{du_S}{dx} = [B_1 + B_2 A_1 + (B_3 + B_2 A_3) C_1] + [B_2 A_2 + (B_3 + B_2 A_3) C_2] \frac{du_G}{dx} \quad [65]$$

in which

$$A_1 = \frac{F_{iG} + F_{gG}}{k_{vG}\epsilon_G \rho_L \{(1 - w_v + w_v \lambda_v) u_G + w_v (1 - \lambda_v) u_L\}} \quad [66]$$

$$A_2 = \frac{\rho_G u_G + k_{vG}\rho_L \{(1 - 2w_v + w_v \lambda_v) u_G + w_v (2 - \lambda_v) u_L\}}{k_{vG}\rho_L \{(1 - w_v + w_v \lambda_v) u_G + w_v (1 - \lambda_v) u_L\}} \quad [67]$$

$$A_3 = \frac{1}{k_{vG}\rho_L \{(1 - w_v + w_v \lambda_v) u_G + w_v (1 - \lambda_v) u_L\}} \quad [68]$$

$$B_1 = -\frac{F_{iS} + F_{gS}}{\epsilon_S u_S (k_{vS}\rho_L + \rho_S)} \quad [69]$$

$$B_2 = \frac{k_{vS}\rho_L u_L}{u_S (k_{vS}\rho_L + \rho_S)} \quad [70]$$

$$B_3 = -\frac{1}{u_S(k_{vS}\rho_L + \rho_S)} \quad [71]$$

$$C_1 = -\frac{F_{wL} + F_{gG} + F_{gL} + F_{gS} + \frac{M_L}{A}A_1 + \frac{M_S}{A}(B_1 + B_2A_1)}{1 + \frac{M_S}{A}A_3 + \frac{M_S}{A}(B_3 + B_2A_3)} \quad [72]$$

$$C_2 = -\frac{\frac{M_G}{A} + \frac{M_L}{A}A_2 + \frac{M_S}{A}B_2A_2}{1 + \frac{M_L}{A}A_3 + \frac{M_S}{A}(B_3 + B_2A_3)} \quad [73]$$

In order to seek the steady-state solutions, the above equations are numerically solved. In order to do so, the solid–gas–liquid three-phase flow region ($L_g \leq x \leq L$) is divided into numerous small parts and three momentum equations are numerically solved in the order of [63], [64] and [65] by using one of the numerical solution techniques for the initial value problem of ordinary differential equations. There are a lot of simple solution methods such as the Runge–Kutta technique and finite difference method etc. In the calculations to be mentioned later, the explicit Euler scheme is adopted. As the result of numerical solutions to the above differential equations, we have the numerical values for P, ρ_G, u_S and u_L at every nodal point. Thus, we can obtain the following values:

$$\epsilon_S = \frac{j_S}{u_S} \quad [74]$$

$$\epsilon_L = \frac{j_L}{u_L} \quad [75]$$

$$\epsilon_G = 1 - \epsilon_L - \epsilon_S \quad [76]$$

$$u_G = \frac{M_G}{A\epsilon_G\rho_G} \quad [77]$$

Incidentally, those numerical results must be unreasonable rather than reasonable because the numerical calculation is performed as the boundary condition with the tentative flow characteristics at the gas-injector. Concretely speaking, the conditions that the velocity of the individual phases is in the order of $u_G > u_L > u_S$, and that the axial velocity gradient $du_k/dx > 0$ (k = G, L, S) for each phase is positive are not always satisfied in the entire range from $x = L_g$ to $x = L$.

We must identify the nearest position from the gas-injector where the axial velocities for each phase are arranged in the order of $u_G > u_L > u_S$ and where the velocity gradients for each phase are positive. By so doing, we can find the eight flow characteristics at the position in the x-direction, and the recalculation is possible by imposing these values to the boundary condition at $x = L_g$. At the same time, it must be checked whether or not the pressure at the outlet section of the upriser reaches P_a (atmospheric pressure). This can be adjusted by the volumetric flux j_L of liquid-phase. At any rate, the three conditions (1) $u_G > u_L > u_S$, (2) $du_k/dx \geq 0$ (k = G, L, S) for each phase and (3) $P = P_a$ must be satisfied. The above numerical procedure is repeated in such a way as to obtain the numerical solution satisfying these conditions.

The numerical procedure mentioned in the next section is very helpful in obtaining the physically justifiable flow characteristics in the entire range from the inlet section of the suction pipe to the outlet section of the upriser.

5. DISCUSSIONS

In order to verify the validity of the present theoretical model based on the multifluid model, the numerical results obtained by this model are compared with the experimental data measured by other researchers. The common numerical values introduced into the calculations are as follows:

$$P_a = 1.0 \times 10^5 \text{ (Pa)}$$

$$T = 293 \text{ (K)}$$

$$R = 287 \text{ (m}^2/(\text{s}^2 \cdot \text{K}))$$

$$\rho_{\text{L}} = 1000 \text{ (kg/m}^3)$$

$$\nu_{\text{L}} = 1.0 \times 10^{-6} \text{ (m}^2/\text{s)}$$

$$g = 9.8 \text{ (m/s}^2)$$

$$\sigma = 7.2 \times 10^{-2} \text{ (N/m)}$$

$$P_0 = P_a + \rho_{\text{L}} g L_s \text{ (Pa)}$$

Firstly, the numerical procedure for introducing the predicted values to be compared with the experimental data will be developed. This has been roughly explained in the previous section. However, in the case of comparing the numerical results with the experimental ones, attention must be paid to that there are some numerical values restricted by the experimental conditions.

Let us now try to compare the numerical values obtained by present model with the experimental data measured by Yoshinaga *et al.* (1990, 1996). They performed experiments using ceramic spheres as the solid particles, and air and water as the working fluids. Their experimental results are expressed by the variation of j_{L} against $j_{\text{G}a}$ with j_{S} as a parameter. Accordingly, $j_{\text{G}a}$ and j_{S} introduced to the boundary values at the position of the air-injector must be unvaried. Since the air volumetric flux $j_{\text{G}a}$ are given and the air density $\rho_{\text{G}a}$ are known at the outlet section of the upriser ($x = L$), the air mass flow rate M_{G} results in being kept constant. Hence, the calculations are performed on condition that both j_{S} and M_{G} are constant.

At the first step of the numerical procedure, the air volumetric fraction $\varepsilon_{\text{G}3}$, the solid volumetric fraction $\varepsilon_{\text{S}3}$ and the liquid volumetric flux j_{L} are given appropriately at any rate. Thus, since the quantities given in [53]–[62] are automatically determined, the flow field in the solid–gas–liquid three-phase mixture region can be calculated. Subsequently, one finds the nearest position from the air-injector satisfying the two conditions that $u_{\text{G}} > u_{\text{L}} > u_{\text{S}}$ and $\text{d}u_k/\text{d}x > 0$ (k = G, L, S) for each phase. The respective volumetric fractions at this position are regarded as those at the air-injector. Again, the calculations in the solid–liquid two-phase flow region are performed and the boundary condition at $x = L_g$ is renewed. By so doing, the flow characteristics in the solid–gas–liquid three-phase flow can be recalculated in the range of $L_g < x \leq L$. However, the case where the pressure at $x = L$ is not equal to the atmospheric pressure ($= P_a$) must occur. This can be adjusted by the liquid volumetric flux j_{L}. However, when j_{L} is changed, the physically unreasonable phenomena may be seen in the numerical calculations. For example, the abnormality of the velocity order and/or the negative velocity gradient may appear in the range from the position of air injection to some location in the x-direction. If such a case occurs, one finds the nearest position from the air injector where $u_{\text{G}} > u_{\text{L}} > u_{\text{S}}$ and $\text{d}u_k/\text{d}x > 0$ (k = G, L, S), and regards the individual volumetric fractions at this position as those at $x = L_g$. Again, the flow characteristics in the two-phase and in the three-phase flow regions can be computed. If the pressure at $x = L$ is not equal to P_a, the pressure adjustment is made by the liquid volumetric flux j_{L}.

In short, the numerical results must satisfy the conditions that $P = P_a$ at $x = L$, $u_{\text{G}} > u_{\text{L}} > u_{\text{S}}$ and $\text{d}u_k/\text{d}x > 0$ (k = G, L, S). This can be achieved by repeating the above-mentioned numerical procedure.

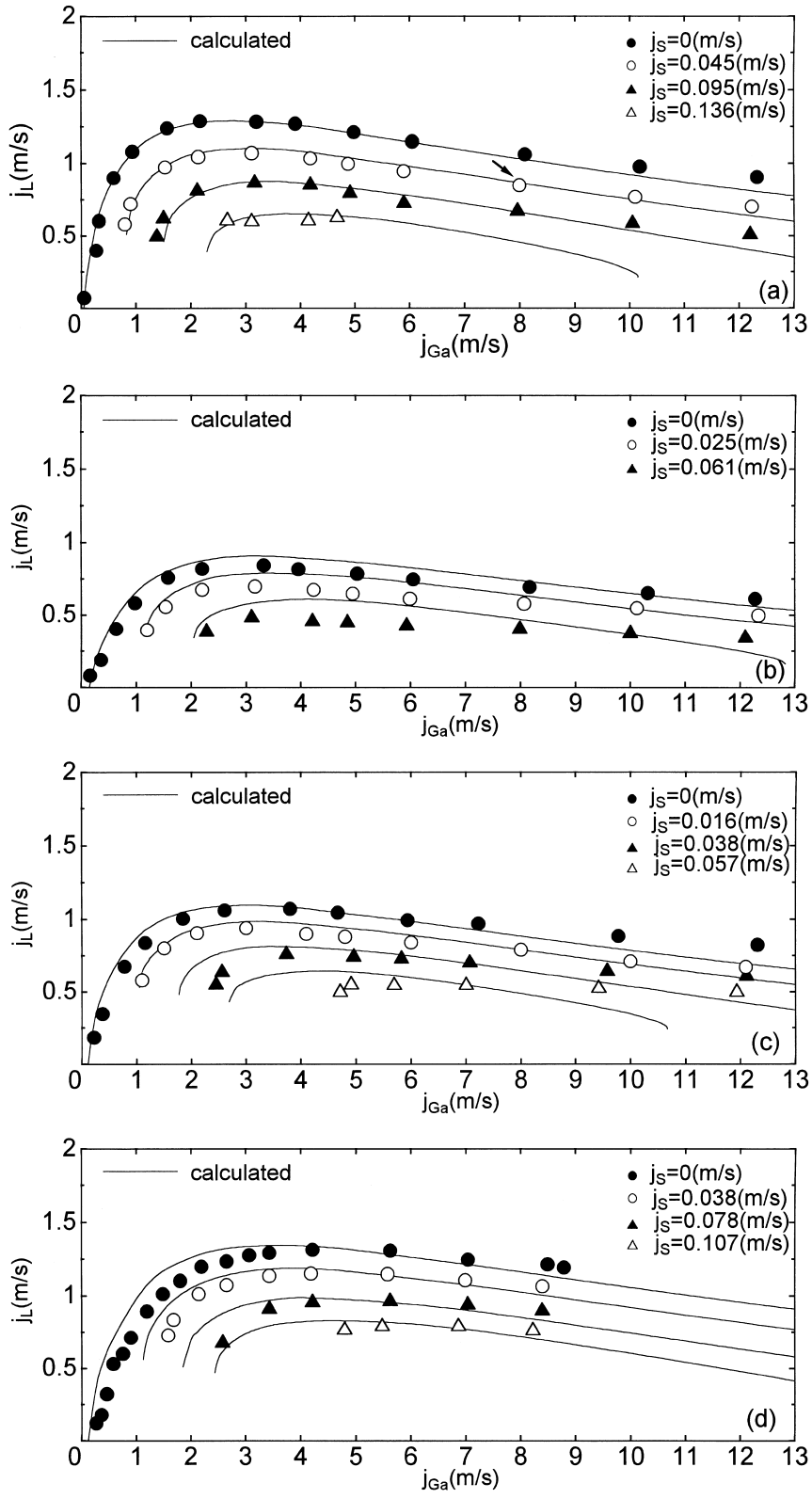
calculated
j_S=0(m/s)
j_S=0.045(m/s)
j_S=0.095(m/s)
j_S=0.136(m/s)
(a)
j_L(m/s)
j_{Ga}(m/s)
calculated
j_S=0(m/s)
j_S=0.025(m/s)
j_S=0.061(m/s)
(b)
j_L(m/s)
j_{Ga}(m/s)
calculated
j_S=0(m/s)
j_S=0.016(m/s)
j_S=0.038(m/s)
j_S=0.057(m/s)
(c)
j_L(m/s)
j_{Ga}(m/s)
calculated
j_S=0(m/s)
j_S=0.038(m/s)
j_S=0.078(m/s)
j_S=0.107(m/s)
(d)
j_L(m/s)
j_{Ga}(m/s)

Fig. 2(a–d).

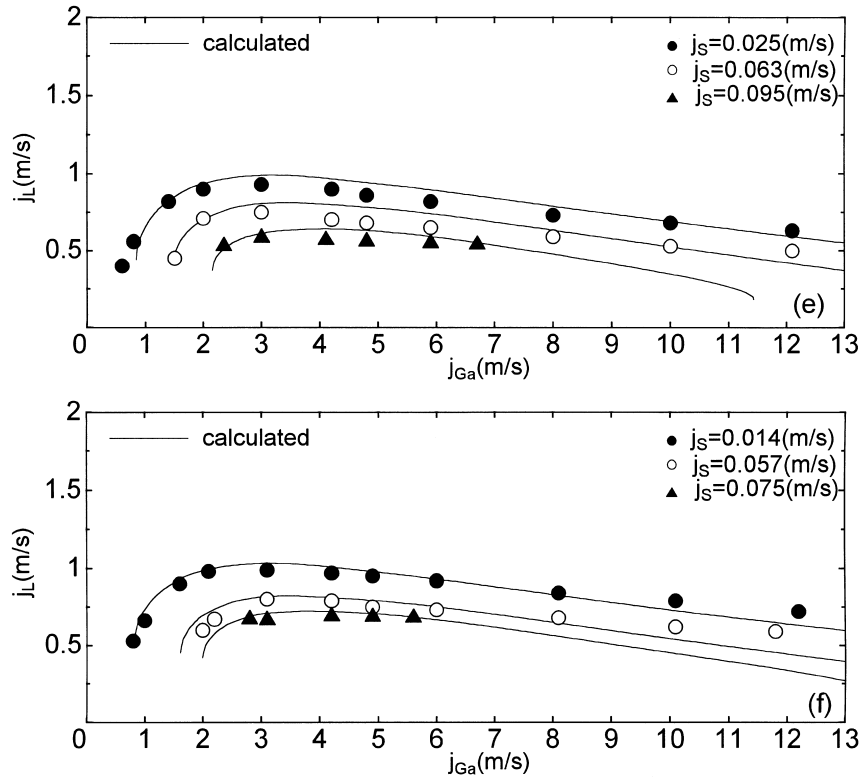

Figure 2. Comparison of numerical results calculated based on present theoretical model with experimental data by Yoshinaga *et al.* (1990, 1996). Experimental conditions of figures (a)–(f) correspond to cases (a)–(f) of table 1, respectively.

Figure 2 (a)–(f) shows the comparisons of the numerical results calculated on the basis of the present theoretical model with the experimental data taken by Yoshinaga *et al.* (1990, 1996). They performed experiments on condition that the inner diameter of pipe is $D = 26$ mm and 40 mm and the submergence ratio defined by

$$\gamma = \frac{L_s - L_g}{L - L_g} \qquad [78]$$

is changed in the range of $\gamma = 0.6$–0.8. And the particles used were ceramic and spherical in shape. The experimental conditions (a)–(f) listed in table 1 correspond to (a)–(f), respectively. The length of the suction pipe L_g is 1.12 m and that of the upriser $L - L_g$ is 6.74 m. Also, the result denoted by the arrow in figure 2(a) will be referred in the later part. They stated that after the air-injection the transitions from the bubble to slug flows and from the slug to churn flows occur. Also, it should be noted that the drag coefficient of solid-phase particle is treated as a function of Re_S and evaluated from [33] because solid particles are spherical in shape. These figures (a)–(f) demonstrate the variation of the liquid volumetric flux j_L against the volumetric

Table 1. List of experimental conditions by Yoshinaga *et al.* (1990,1996)

Case	γ	D(mm)	ρ_S(kg/m^3)	d_S (mm)
(a)	0.8	26	2540	6.12
(b)	0.6	26	2540	6.12
(c)	0.7	26	3630	6.00
(d)	0.7	40	2540	9.92
(e)	0.7	26	2540	6.1
(f)	0.7	26	2540	9.9

flux j_{Ga} of supplied air reduced to the atmospheric state with the solid volumetric flux j_S as a parameter. The calculated values shown by solid lines give good agreement with the experiments.

Figure 3 (a) and (b) indicates the flow characteristics calculated on condition that $j_{Ga} = 8.0$ m/s and $j_S = 0.045$ m/s. This corresponds to the experimental value shown by the arrow in figure 2(a). Therefore, the computation has been performed in accordance with the above mentioned experimental condition (see case (a) in table 1). Figure 3(a) gives the steady-state velocity rising in a pipe for each phase. The left side of the dotted line corresponds to the solid–liquid two-phase flow region and the right side does to the solid–gas–liquid three-phase region. The velocity for each phase, of course, remains unchangeable in the solid–liquid two-phase flow region. At the air-injection point, the velocity jump of u_S and u_L occurs owing to injecting air into the upriser through an air-injector. Also, in the solid–gas–liquid three-phase flow region, the order of the velocity magnitude is kept in the state of $u_G > u_L > u_S$ and the velocity gradient for each phase increases slowly along the x-axis. Figure 3(b) indicates the variation of the volumetric fraction for each phase and of pressure with x. In the two-phase region, the both volumetric fractions are kept constant, and ε_L is much higher than ε_S. At the air-injector, ε_L and ε_S are seen to drop rapidly owing to injecting air into the pipe. Also, in the three-phase region, the volumetric fraction ε_G of gas-phase increases gradually along the x-axis, while ε_L and ε_S decrease slowly. In addition, the pressure gradient is seen to be sharper in the two-phase flow region than that in the three-phase flow region. The pressure at the outlet section of the upriser ($L = 7.86$ m) reaches the atmospheric one P_a. Furthermore, it is seen that $\varepsilon_G > 0.8$ in the entire three-phase flow region. This suggests that the churn flow pattern is maintained and no transition occurs throughout this region.

Here we attempt to compare the numerical values calculated on the basis of the present theoretical model with the experiments performed by Kawashima *et al.* (1975). They performed the

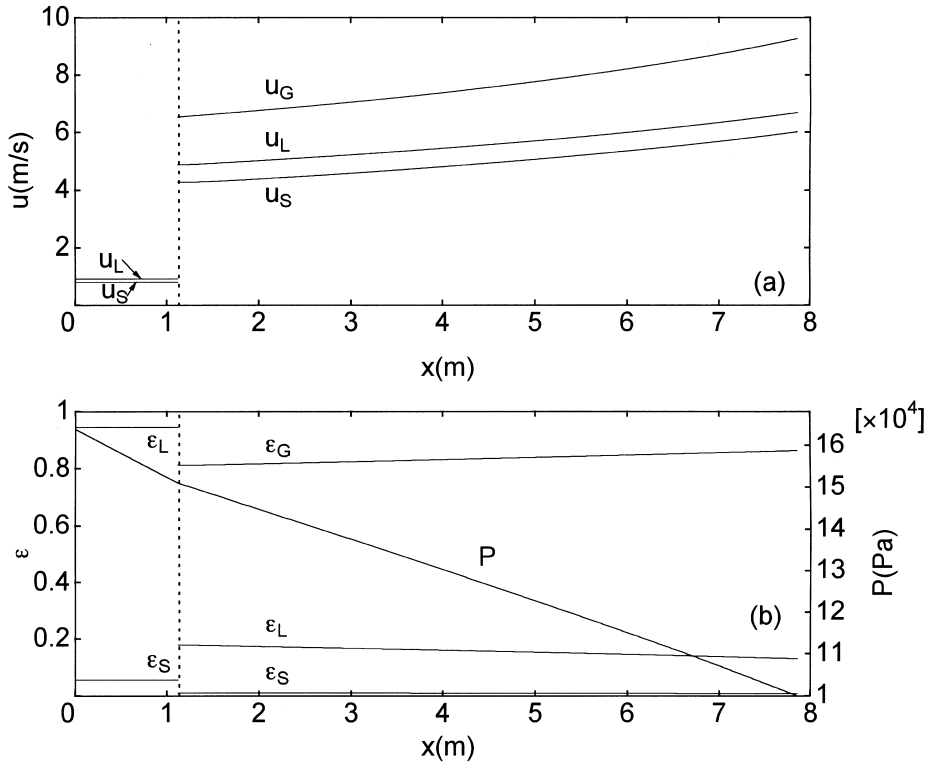

Figure 3. Variation of velocity rising in a pipe for each phase (a), and variation of volumetric fraction for each phase and of pressure with x and (b) for the case where $j_{Ga} = 8.0$ m/s and $j_S = 0.045$ m/s which corresponds to the experimental value shown by an arrow in figure 2(a).

experiments on an air-lift pump using the pipe of inner diameter $D = 50$ mm and the length $L = 6.0$ m. The solid particles are gravel and not spherical in shape. The diameter of equivalent sphere after reduction on the assumption that particle is spherical body with the same volume and the same density is $d_S = 1.73$ mm and the density ρ_S is (2670 kg/m^3). The drag coefficient measured by them is $C_{DS} = 2.44$. The submergence ratio γ is set to 0.92. The length of the suction pipe is negligibly small ($L_g \simeq 0$).

Figure 4 gives the relation between the experimental data and the calculated values. The calculations have been performed in accordance with the experimental condition mentioned above. Also, the presentation of the experimental results is the same as their original paper. The parameter β_s appearing in this figure is the volumetric concentration of particles discharged at the outlet section of the upriser, defined by

$$\beta_s = \frac{j_S}{j_L + j_S} \qquad [79]$$

It may be accepted from this figure that the numerical results calculated on the basis of the present theoretical model give best-fit to the experimental data.

Next, we will consider the comparison of the numerical results with the experiments performed by Usami and Saito (1986). They performed the experiments by lifting simulated manganese nodules of the equivalent sphere diameter $d_S = 36.3$ mm and the density $\rho_S = 1960$ (kg/m^3) in a lifting pipe of $D = 155.4$ mm and $L = 32.63$ m. In their experiments, L_g is 4.96 m and γ is 0.82. Also, they reported that the measured value of the drag coefficient for solid particles C_{DS} is 1.03.

Figure 5 gives the comparison between the experimental and theoretical values. The parameter β_s in this figure denotes the volumetric concentration of particles discharged defined by [79]. Although it can be imagined that the aim of this experiment is to confirm the relation between j_{Ga} and j_S on condition that β_s holds constant, it is very difficult to explicitly understand from such experimental results the variation of the solid volumetric flux j_S in a wider range of j_{Ga}. It may be not appropriate that β_s is given by a section such as $\beta_s = 0.063$–0.066 even for the case of only two experimental values. At any rate, the present calculations give good agreement with the experimental data.

Furthermore, we tried to compare the numerical results with the experiments performed by Saito *et al.* (1986). They made a study on the operation performance of an air-lift pump on con-

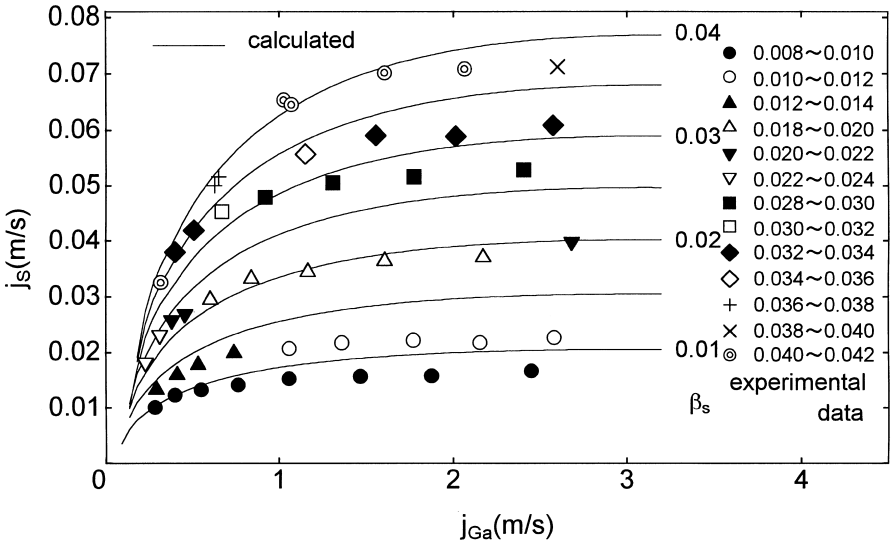

Figure 4. Comparison of numerical results with experimental data by Kawashima *et al.* (1975). Note that β_s is defined by [79].

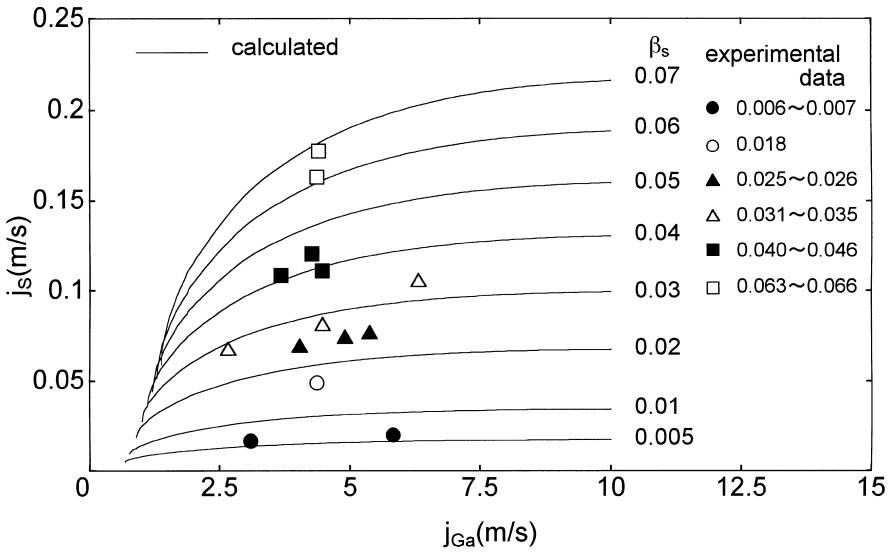

Figure 5. Comparison of numerical results with experimental data by Usami *et al.* (1986). Note that β_s is defined by [79].

dition that simulated manganese modules of $d_S = 42.3$ mm and $\rho_S = 1990$ (kg/m^3) are conveyed upward in a vertical pipe of $D = 151$ mm and $L = 196.6$ m. They reported that the measured drag coefficient $C_{DS} = 0.84$, the submergence ratio $\gamma = 0.936$ and the length of the suction pipe $L_g = 16$ m.

Yoshinaga *et al.* (1990) attempted to compare the numerical results calculated on the basis of their own numerical model with the experimental data measured on the above mentioned condition for the two cases where $\beta_s = 0$ and $\beta_s = 0.06$–0.07. Accordingly, we will also compare the numerical results with the above-mentioned experimental ones. The comparison is shown in figure 6. The expression of this figure is the same as the original paper by Yoshinaga *et al.* (1990). The calculation shown by solid lines is based upon the present model and the calculation by dotted lines is shown in the model by Yoshinaga *et al.* (1990). Apart from discussing the quality of two kinds of numerical results, the numerical results calculated on the basis of the

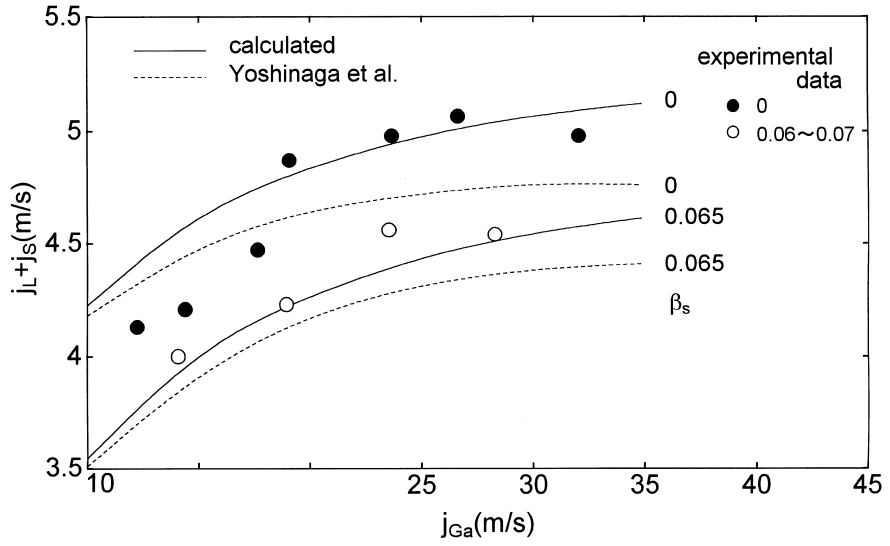

Figure 6. Comparison of numerical results with experimental data by Saito *et al.* (1986). The calculation shown by solid lines is based upon the present model and the calculation by dotted lines is based upon the model built up by Yoshinaga *et al.* (1990).

present theoretical model can be regarded to be in good agreement with the experimental ones, in spite of scattering in the experimental data.

Finally, we will attempt to compare the numerical results with the experiments performed by Weber and Dedegil (1976). They performed the experiments using a large-scale air-lift pump to convey gravel. The pipe diameter is $D = 300$ mm, and three kinds of solid particles are used. Table 2(a) denotes their experimental conditions and results for the case where $\rho_S = 2575$ kg/m^3, $d_S = 5$ mm and $C_{DS} = 1.20$. Table 2(b) denotes those for the case where $\rho_S = 2610$ kg/m^3, $d_S = 0.6$ mm and $C_{DS} = 2.05$, and table 2(c) corresponds to the case whose $\rho_S = 1143$ kg/m^3, $d_S = 50$ mm and $C_{DS} = 1.17$.

Figure 7(a) demonstrates the comparison between the experimental volumetric flux $j_{S,\,exp}$ and theoretical solid volumetric flux $j_{S,\,cal}$. The empty circle, solid circle and triangle corresponds to table 2(a), (b) and (c), respectively. The present calculations are seen to be in fairly good agreement with the experimental data.

Figure 7 (b) gives the variation of j_L against j_{Ga} in the gas–liquid two-phase flow. The empty and solid circles in this figure denote the experimental data measured by them and the solid line indicates the theoretical results calculated on the basis of the present model. The present calculations are seen to give good fit to the experimental data.

We will discuss the existing region of numerical solutions from a practical point of view. Figure 8 indicates the numerical solutions obtained on the same condition as the experiments performed by Yoshinaga *et al.* (1990) (see figure 2(a)). The solutions are seen to exist on a closed curve, in which the upper and lower curve are shown by solid and dotted lines, respectively. It is noted that the points A, B, X and Y will be referred in later part. Taking the case of

Table 2. Experimental conditions and results performed by Weber *et al.* (1976) for the cases where (a) (ρ_S, d_S, C_{DS} = (2575 kg/m^3, 5 mm, 1.20) (b) (2610 kg/m^3, 0.6 mm, 2.05) and (c) (1143 kg/m^3, 50 mm, 1.17), respectively.

No.	L(m)	L_g(m)	γ	j_{Ga} m/s	j_S m/s	β_s
			(a)			
1	55.4	6.2	0.8537	8.135	0.1697	0.0447
2	55.4	6.2	0.8537	5.517	0.0963	0.0267
3	55.4	6.2	0.8537	3.301	0.0755	0.0269
4	279.0	101.0	0.9607	2.641	0.0285	0.0113
5	282.0	101.0	0.9613	3.631	0.0632	0.0229
6	285.0	101.0	0.9620	5.423	0.0807	0.0339
7	288.0	101.0	0.9626	5.730	0.1350	0.0395
8	294.0	101.0	0.9637	3.678	0.0530	0.0189
9	324.0	101.0	0.9686	3.513	0.0547	0.0217
10	325.9	101.0	0.9693	5.612	0.1177	0.0406
11	329.9	101.0	0.9699	4.645	0.1091	0.0370
12	332.9	101.0	0.9702	3.395	0.0583	0.0251
13	407.6	290.0	0.9439	5.282	0.0788	0.0430
14	449.7	290.0	0.9518	3.702	0.0362	0.0149
15	449.8	197.0	0.9731	7.215	0.1325	0.0446
16	450.3	197.0	0.9712	5.187	0.0766	0.0258
			(b)			
1	257.3	4.9	0.9746	3.560	0.0778	0.0264
2	261.3	4.9	0.9672	5.517	0.1791	0.0710
3	261.3	4.9	0.9672	6.461	0.1720	0.0640
4	357.4	101.0	0.9672	5.022	0.1601	0.0601
5	357.4	101.0	0.9672	6.909	0.1528	0.0589
6	357.9	101.0	0.9654	3.112	0.0732	0.0325
7	449.4	197.0	0.9707	6.838	0.1056	0.0386
			(c)			
1	449.3	197.0	0.9711	7.026	0.2094	0.0470
2	449.3	296.0	0.9524	7.451	0.2998	0.0780
3	449.4	197.0	0.9707	5.494	0.1806	0.0470
4	449.4	197.0	0.9707	7.144	0.2215	0.0540
5	449.8	290.0	0.9574	9.785	0.3589	0.0860
6	451.0	341.0	0.9364	5.824	0.1652	0.0480
7	451.0	341.0	0.9364	8.252	0.2377	0.0600
8	451.0	341.0	0.9364	10.092	0.2865	0.0750

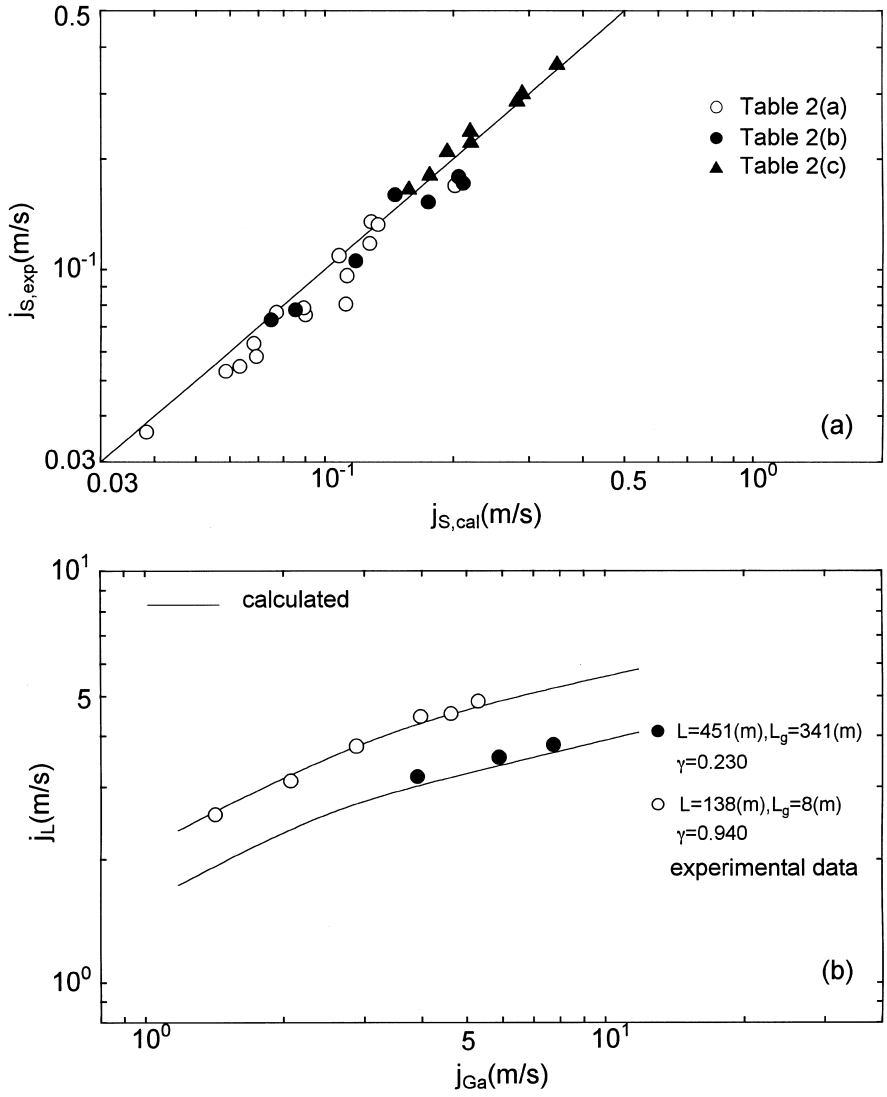

Figure 7. (a) Comparison between experimental solid volumetric flux $j_{S,exp}$ by Weber *et al.* (1976) and theoretical flux $j_{S,cal}$, and (b) comparison of experimental relation between j_L and j_{Ga} with theoretical one in gas-liquid two-phase flow.

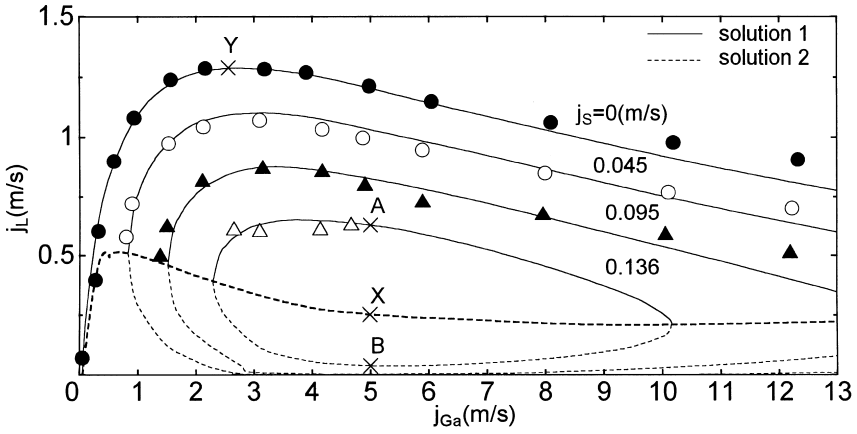

Figure 8. Solution curves to governing equations for case (a) in table 1. Note that the upper solution is shown by solid lines and the lower solution is done by the dotted lines, respectively. A thick dotted line denotes the boundary between the solid and dotted lines.

$j_S = 0.136$ m/s for example, the closed curve where the numerical solutions exist is divided into two parts by a thick dotted line and the upper and lower curves agree with each other at both ends. Again, the existing region of solutions expands and the closed curve enlarges itself with the decrease in j_S. Only the upper curve exists and the lower curve disappears at $j_S = 0$ m/s. Namely, the numerical solution of j_L for $j_S = 0$ m/s is reduced to a single value for j_{Ga}. As can be understood from this figure, the experimental data are concentrated on the upper part of the closed curve. At any rate, it has been demonstrated that the numerical solution to the governing equations have the two values, if $j_S \neq 0$ m/s.

Let us now consider the difference between the two numerical solutions for the case where $j_S = 0.136$ m/s and $j_{Ga} = 5.0$ m/s. Figure 9(a) and (b) indicates the variation of the rising velocity and volumetric fraction for each phase along a vertical pipe. The two points denoted by A and B are the numerical solutions shown in figure 8. What is noticeable in figure 9(b) is that for the solution A the volumetric fraction of liquid-phase is always larger than that of solid-phase. But, the case of the solution B is the reverse. It is self-evident that the solution B is not realistic.

We will consider why there are two different solutions on the same condition. Figure 10(a) indicates the variation of pressure along the vertical pipe. Although it can be seen that the pressure at the bottom and top ends of the pipe is the same between the two solutions A and B, the pressure distribution from the bottom to the top ends is different between the two. In the two-phase flow region, the pressure gradient of the case B is steeper than that of the case A, but in the three-phase flow region, the former becomes more gradual than the latter.

Figure 10(b) denotes the variation of the respective forces per unit volume in the two- and three-phase regions. Here, F_w, F_g and F_a are defined by

$$F_w = F_{w\mathrm{L}} \tag{80}$$

$$F_g = F_{g\mathrm{G}} + F_{g\mathrm{L}} + F_{g\mathrm{S}} \tag{81}$$

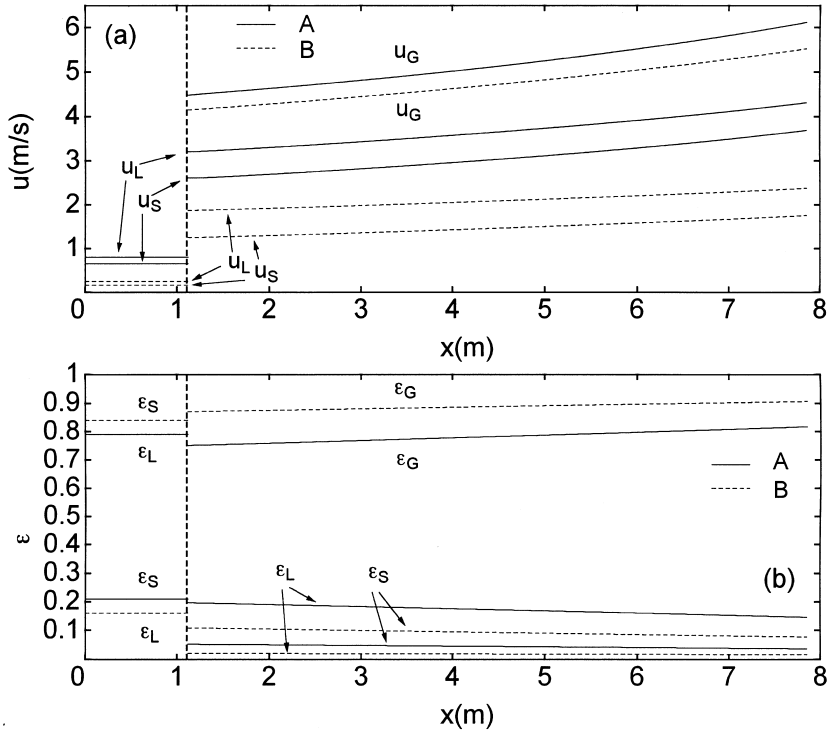

Figure 9. (a) Variation of rising velocity and (b) volumetric fraction for each phase along a vertical pipe for the case where $j_S = 0.136$ m/s and $j_{Ga} = 5.0$ m/s. Note that the solid and dotted lines denote the numerical solution at points of *A* and *B* in figure 8, respectively.

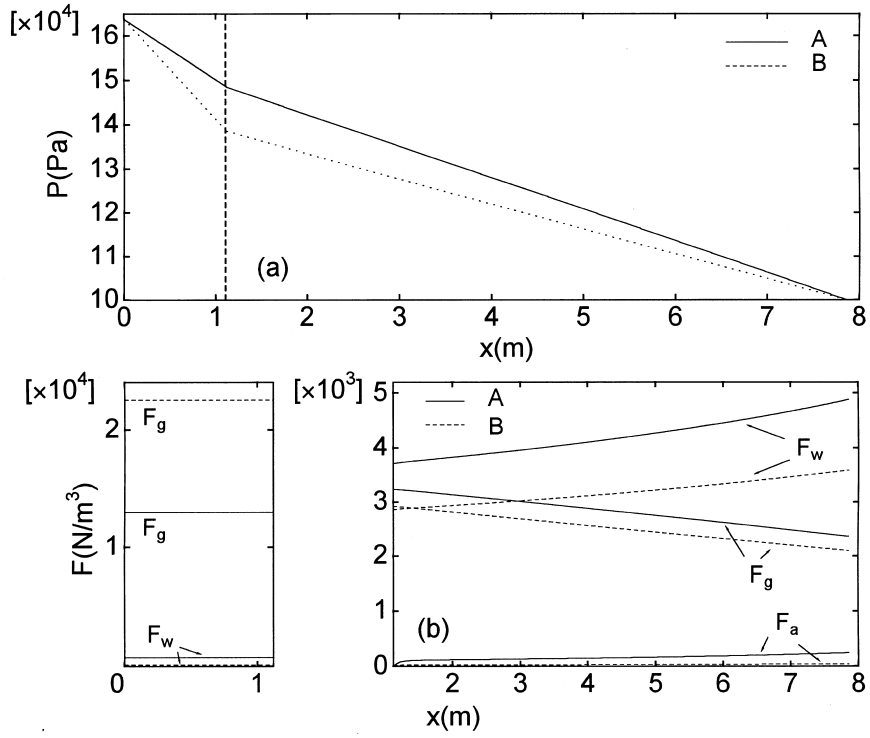

Figure 10. (a) Variation of pressure along a vertical pipe, and (b) variation of respective forces (see [80]–[82]) per unit volume in two- and three-phase regions for case where $j_S = 0.136$ m/s and $j_{Ga} = 5.0$ m/s. Note that the solid and dotted lines denote the solution at points of A and B in figure 8, respectively.

$$F_a = \left(M_G \frac{du_G}{dx} + M_L \frac{du_L}{dx} + M_S \frac{du_S}{dx} \right) \frac{1}{A} \qquad [82]$$

Accordingly, the negative value of the sum of the three kinds of forces corresponds to the pressure gradient

$$\frac{dP}{dx} = -F_w - F_g - F_a \qquad [83]$$

which can be easily derived by [4]–[6]. Attention must be paid to that $F_{gG} = 0$ N/m^3 and $M_G = 0$ kg/s in the two-phase flow region. In the figure 10(b), one can see that the gravity force F_g of the case B is much larger than that of the case A in the two-phase flow region. This is based upon the difference in the solid volumetric fractions between both cases A and B. Namely, in the case B, ε_S is much larger in the two-phase flow region than ε_L, as shown in figure 9(b). This fact leads to the sharpness of the pressure gradient of the case B in the two-phase flow region.

In the three-phase flow region, both F_g and F_w of the case A are kept always larger than those of the case B, respectively. These results are owing to the fact that the gas volumetric fraction of the case B is kept larger than that of the case A. F_g decreases along the x-axis for both cases A and B. This is due to the increase in the gas volumetric fraction as the three-phase mixture flows upward in the upriser. Also, the friction force F_w of the case A is larger than that of the case B. This is because the superficial mixture velocity u_m (see [43]) of the case A is larger than that of the case B, as shown in figure 9(a). F_w increase with the x-axis for both cases A and B, because u_m becomes larger with x. The sum of the respective inertial forces F_a is very small in comparison to F_g and F_w. At any rate, in contrast to the case of two-phase flow region, we find that the pressure gradient of the case A is steeper in the three-phase region than that of the case B.

Eventually, it has been confirmed that the presence of the two numerical solutions is based upon the fact that two sets of flow characteristics entirely different in both the two- and three-phase flow regions can be obtained numerically. However, the fact that $\varepsilon_S > \varepsilon_L$ in the two- and three-phase flow regions can not occur from a phenomenal point of view.

Finally, we consider theoretically the maximum amount of the solid particles to be lifted. Figure 8 shows that the existing region of the numerical solution becomes small with the increase in j_S. The upper and lower limits are approachable on through the thick dotted line as j_S is increased. And the upper limit coincides with the lower one on the boundary line at a certain value of $j_{S,\ max}$. That is, it is suggested that the numerical solution is not present in the range of $j_S > j_{S,max}$. This corresponds to the theoretical value of the maximum volumetric flux of the solid particles. By the way, the point X, as shown in figure 8, denotes the solution satisfying this condition and $j_{S,max} = 0.18$ m/s in this case. Next, the theoretical maximum value $j_{L,max}$ of the liquid volumetric flux to be lifted, of course, corresponds to the case where $j_S = 0$ m/s and $j_{L,max} = 1.28$ m/s in the present case (see the point Y in figure 8).

6. CONCLUSION

This paper has treated the theoretical analysis to predict the steady-state flow characteristics of the air-lift pump for the case where a transition from the solid–liquid two-phase flow to the solid–gas–liquid three-phase flow occurs by injecting gas-phase into a vertical pipe through a gas-injector. The system of governing equations is based upon the multifluid model. The transitions of the flow pattern of gas-phase are taken into consideration in the system of equations governing the solid–gas–liquid three-phase flow. Therefore, even though the flow pattern transition from the bubbly flow to the slug flow as well as from the slug flow to the churn flow occurs, the flow characteristics peculiar to the multiphase flow can be obtained from qualitative and quantitative points of view. In order to verify the validity of the system of governing equations accounting for the transitions of the gas flow pattern, the results calculated on the basis of the present theoretical model have been compared to the experimental results obtained by several other researchers. We have found that the theoretical model built up in the present investigation gives best-fit to the prediction of the operation performance of an air-lift pump. Furthermore, we have concretely demonstrated that the present theoretical model on the basis of the multifluid model is capable of predicting the maximum solid/liquid volumetric flux.

Here the emphasis has been placed upon obtaining the steady-state flow characteristics, because all of the experimental data to be compared with the calculation were taken on the steady-state condition. We would like to add to note that the system of equations constructed here can be extended to obtaining the transitional numerical solutions, although it is very difficult to establish the transitional situation of the multiphase flow in a pipe.

Acknowledgements—The authors would like to note that this study was supported through a Grant-in-Aid for Scientific Research (A) (07555519) from the Ministry of Education, Science, Sports and Culture in Japan.

REFERENCES

Drew, D., Cheng, L. and Lahey, R. T. Jr (1979) The analysis of virtual mass effects in two-phase flow. *Int. J. Multiphase Flow* **5,** 233–242.

Fujimoto, H., Isobe, M., Fukui, Takashi and Hatta, Natsuo (1997) Effect of pressure drop owing to friction between pipe inner wall and water on non-equilibrium flow fields in an air-lifting pipe-4th report. *Shigen-to-Sozai* **113,** 133–139 (in Japanese).

Griffith, P. and Wallis, G. B. (1961) Two-phase slug flow. *Transaction of the ASME Section-C* **83,** 307–320.

Hatta, N. and Fujimoto, H. (1996) Theoretical analysis for non-equilibrium flow fields with transitional process from two-phase to three-phase mixtures by injecting air halfway into a lifting Pipe-3rd report. *Shigen-to-Sozai* **112,** 81–88 (in Japanese).

Hewitt, G. F. and Hall-Taylor, N. S. (1970) *Annular Two-phase Flow*. Pergamon Press.

Hinze, J. O. (1962) Momentum and mechanical-energy balance equations for a flowing homogeneous suspension with slip between the two phases. *Appl. Sci. Res. Section-A* **2,** 33–46.

Ishii, M. (1977) *One-dimentional Drift-flux Model and Constitutive Equations for Relative Motion Between Phases in Various Two-phase Flow Regimes*. Argonne National Laboratory.

Ishii, M., Mishima, K., Kataoka, I. and Kocamustafaogullari, G. (1982) Two-fluid model and importance of the interfacial area in two-phase flow analysis. *Proc. 9th U.S. National Congress of Applied Mechanics*. Ithaca, New York. pp. 73–80.

Kamata, C. and Ito, K. (1995) Cold model experiments on the application of gas lift pump to the transportation of molten metal. *ISIJ International* **35,** 859–865.

Kawashima, T., Noda, K., Masuyama, T. and Oda, S. (1975) Hydraulic transport of solids by air lift pump. *J. Mining Metall. Inst. Japan* **91,** 765–772 (in Japanese).

Kocamustafaogullari, G., Huang, W. D. and Razi, J. (1994) Measurement and modeling of average void fraction, bubble size and interfacial area. *Nucl. Eng. and Des.* **148,** 437–453.

Kurul, N. and Podowski, M. Z. (1991) *ANS Proc. 1991, National Heat Transfer Conference*. Minneapolis.

Lahey, R. T., Cheng, L. Y., Drew, D. A. and Flaherty, J. E. (1980) The effect of virtual mass on the numerical stability of accelerating two-phase flows. *Int. J. Multiphase Flow* **6,** 281–294.

Ransam, V. H. *et al.* (1981) *RELAP 5/MOD 1 Code Manual, Volume 1, System Models and Numerical Methods*. NUREG/CR-1826.

Sadatomi, M., Sato, Y., Yoshinaga, T. and Inagaki, K. (1990a) Hydraulic lifting of coarse particles in vertical pipes—1st report, liquid–solid two-phase flow. *Jap. J. Multiphase Flow* **4,** 111–124 (in Japanese).

Sadatomi, M., Sato, Y., Yoshinaga, T. and Maeda, S. (1990b) Hydraulic lifting of coarse particles in vertical pipes—2nd report, gas–liquid–solid three-phase flow. *Jap. J. Multiphase Flow*. **4**, 125–140 (in Japanese).

Saito, T., Tomishima, Y., Yamasaki, T., Usami, T., Yokokawa, A. and Shimizu, Y. (1986) Lifting characteristics of manganese nodules by air lift pump under steady conditions—1st report, fundamental results of 200 m test plant. *Saiko-to-Hoan* **32,** 540–551 (in Japanese).

Taitel, Y., Barnea, D. and Dukler, A. E. (1980) Modelling flow pattern transitions for steady upward gas–liquid flow in vertical tubes. *AIChE J.* **26,** 345–354.

Tomiyama, A., Kataoka, I. and Sakaguchi, T. (1995) Drag coefficients of bubbles—1st report, drag coefficients of a single bubble in a stagnant liquid. *Transactopn of the JSME Section-B* **61,** 2357–2364 (in Japanese).

Tomiyama, A., Kataoka, I., Fukuda, T. and Sakaguchi, T. (1995) Drag coefficients of bubbles—2nd report, drag coefficient for a swarm of bubbles and its applicability to transient flow. *Transactopn of the JSME Section-B*. 61. 2810–2817. (in Japanese).

Usami, T. and Saito, T. (1986) Studies on the hydraulic lifting of solids by air-lift pump. *Report of the National Research Institute for Pollution and Resources*, 1–104 (in Japanese).

Wallis, G. B. (1969) *One-dimensional Two-phase Flow*. McGraw-Hill, New York.

Weber, M. and Dedegil, Y. (1976) *Hydrotransport 4*., pp. H1–1–H1-23.

Yoshinaga, T., Sato, Y. and Sadatomi, M. (1990) Characteristics of air-lift pump for conveying solid particles. *Jap. J. Multiphase Flow*. 4, pp. 174–191 (in Japanese).

Yoshinaga, T. and Sato, Y. (1996) Performance of an air-lift pump for conveying coarse particles. *Int. J. Multiphase Flow* **22,** 223–238.

Zuber, N. (1967) Flow excursions and oscillations in boiling, two-phase flow systems with heat addition. *Proceedings of EURATOM Symposium on Two-phase Flow Dynamics* **1,** 1070–1089.